PNAS RESEARCH ARTICLE | MICROBIOLOGY OPEN ACCESS

A highly efficacious live attenuated mumps virus–based SARS-CoV-2 vaccine candidate expressing a six-proline stabilized prefusion spike

Yuexiu Zhang[a,1], Mijia Lu[a,1], K C Mahesh[b,1], Eunsoo Kim[a,2], Mohamed M. Shamseldin[c,2], Chengjin Ye[d,2], Piyush Dravid[b,2], Michelle Chamblee[a,2], Jun-Gyu Park[d], Jesse M. Hall[c], Sheetal Trivedi[b], Supranee Chaiwatpongsakorn[b], Adam D. Kenny[c], Satyapramod Srinivasa Murthy[b], Himanshu Sharma[b], Xueya Liang[a], Jacob S. Yount[c,e], Amit Kapoor[b,e,f], Luis Martinez-Sobrido[d], Purnima Dubey[c,e], Prosper N. Boyaka[a,e], Mark E. Peeples[b,e,f], and Jianrong Li[a,e,3]

Edited by Diane Griffin, Johns Hopkins University, Baltimore, MD; received February 1, 2022; accepted April 24, 2022

With the rapid increase in SARS-CoV-2 cases in children, a safe and effective vaccine for this population is urgently needed. The MMR (measles/mumps/rubella) vaccine has been one of the safest and most effective human vaccines used in infants and children since the 1960s. Here, we developed live attenuated recombinant mumps virus (rMuV)–based SARS-CoV-2 vaccine candidates using the MuV Jeryl Lynn (JL2) vaccine strain backbone. The soluble prefusion SARS-CoV-2 spike protein (preS) gene, stablized by two prolines (preS-2P) or six prolines (preS-6P), was inserted into the MuV genome at the P–M or F–SH gene junctions in the MuV genome. preS-6P was more efficiently expressed than preS-2P, and preS-6P expression from the P–M gene junction was more efficient than from the F–SH gene junction. In mice, the rMuV-preS-6P vaccine was more immunogenic than the rMuV-preS-2P vaccine, eliciting stronger neutralizing antibodies and mucosal immunity. Sera raised in response to the rMuV-preS-6P vaccine neutralized SARS-CoV-2 variants of concern, including the Delta variant equivalently. Intranasal and/or subcutaneous immunization of IFNAR1$^{-/-}$ mice and golden Syrian hamsters with the rMuV-preS-6P vaccine induced high levels of neutralizing antibodies, mucosal immunoglobulin A antibody, and T cell immune responses, and were completely protected from challenge by both SARS-CoV-2 USA-WA1/2020 and Delta variants. Therefore, rMuV-preS-6P is a highly promising COVID-19 vaccine candidate, warranting further development as a tetravalent MMR vaccine, which may include protection against SARS-CoV-2.

SARS-CoV-2 | mumps virus | vaccine

Significance

An efficacious pediatric SARS-CoV-2 vaccine is needed to halt the current pandemic. Mumps virus (MuV) vaccine is one of the safest and most efficient vaccines with a track record in children. Here, we developed recombinant MuV (rMuV)–based SARS-CoV-2 vaccine candidates expressing a stabilized prefusion spike with two prolines (preS-2P) or six prolines (preS-6P) at different gene junctions in the MuV genome. Among them, rMuV-based preS-6P vaccine candidates induce robust neutralizing antibodies, mucosal immunoglobulin A antibodies, and T cell immune responses, and provides complete protection against challenge with SARS-CoV-2 WA1 and Delta variants. The preexisting MuV immunity has a minimal impact on generating SARS-CoV-2–specific immune responses. Thus, rMuV-preS-6P is a highly efficacious SARS-CoV-2 vaccine candidate in current small-animal models.

The current pandemic of severe acute respiratory syndrome coronavirus 2 (SARS-CoV-2) has caused tremendous damage to all aspects of our society (1–3). As of 1 June 2022, nearly 528 million cases have been reported worldwide, with nearly 6.3 million deaths (~1.20% mortality). Symptoms of SARS-CoV-2 infection are primarily respiratory although increasing numbers of other syndromes such as cognitive deficits are being reported. As of June 2022, several SARS-CoV-2 vaccines based on messenger RNA (mRNA), inactivated virus, and adenovirus vectors (Ad26.COV2.S and ChAdOx1) have been approved for vaccination in humans over the age of 5 (4). These vaccines are highly efficacious, reaching 70 to 95% effectiveness against SARS-CoV-2 infection (4).

Despite the high success of the current SARS-CoV-2 vaccines, there are several limitations. Protection provided by current vaccines begins to decline after 3 mo (5), which has required a third or fourth dose to boost the immune response. Current vaccines are less effective against recently emergent SARS-CoV-2 variants of concern (VoCs) (6–9). More and more evidence has shown that vaccine-induced neutralizing antibodies were significantly weakened or insufficient to neutralize VoCs such as the Delta variant (7–9), which spreads much faster and causes more severe illness than the earlier strains. In addition, the current vaccines neutralize the most recently emerged variant, Omicron, ~40 times less efficiently compared with early SARS-CoV-2 isolates (10, 11). The mRNA vaccines are expensive to produce, hard to transport internationally, and difficult to store in many countries because of the requirement for expensive −80 °C freezers.

A safe and efficacious pediatric SARS-CoV-2 vaccine is needed to halt the current pandemic. Pfizer's mRNA vaccine is 90.7% effective in preventing COVID-19 symptoms in children 5 to 11 y old (12, 13). On 17 June 2022, Food and Drug Administration (FDA) authorized emergency use of the Moderna and Pfizer mRNA vaccines for children down to 6 mo of age. As of 23 June 2022, a total of 13.7 million COVID-19 cases have occurred in children, representing 18.8% of the total COVID-19 cases in the

Competing interest statement: The Ohio State University Research Foundation and Abigail Wexner Research Institute at Nationwide Children's Hospital have filed an invention report for the mumps virus–based SARS-CoV-2 vaccine.

This article is a PNAS Direct Submission.

[1]Y.Z., M.L., and M.K.C. contributed equally to this work.

[2]E.K., M.M.S., C.Y., P. Dravid, and M.C. contributed equally to this work.

[3]To whom correspondence may be addressed. Email: li.926@osu.edu.

This article contains supporting information online at http://www.pnas.org/lookup/suppl/doi:10.1073/pnas.2201616119/-/DCSupplemental.

Published July 27, 2022.

United States. Notably, COVID-19 cases in children have increased significantly after the reopening of schools. Therefore, development of other vaccine platforms and strategies to enhance durability, reduce cost, and enhance stability are essential for terminating the pandemic.

Historically, the MMR (measles/mumps/rubella) vaccine has been one of the safest and most effective human vaccines ever developed (14–16). The application in children started in the 1960s and provides long-lasting protection against these three viruses (14, 16). Among the three MMR components, measles virus (MeV) and mumps virus (MuV) are nonsegmented negative-sense (NNS) RNA viruses, belonging to the family *Paramyxoviridae* in the order *Mononegavirales*. The MuV genome is 15,384 nt in length, and it encodes seven structural proteins arranged in the order 3′-leader-N-P-M-F-SH-HN-L-trailer-5′ (17). The limited number of discrete genes of the NNS RNA genome and the intergenic regions available for inserting additional genes facilitates the development of live vectored vaccines. MuV is an excellent viral vector for delivery of vaccines against other highly pathogenic viruses, primarily because of its high safety and efficacy, well-established good manufacturing practices, induction of long-lived immunity, and the potential for the development of a quadrivalent vaccine against four major pediatric diseases (18, 19).

In this study, we developed a suite of safe and highly efficacious recombinant MuV (rMuV)–based SARS-CoV-2 vaccine candidates expressing a stabilized prefusion spike with two prolines (preS-2P) or six prolines (preS-6P) at different gene junctions in the MuV genome. Among them, the rMuV-based preS-6P vaccine induces a broad neutralizing antibody against VoCs and T cell immunity, and provides complete protection against SARS-CoV-2 WA1 and the Delta variant challenge in animal models.

Results

Recovery and Characterization of rMuV Expressing a Prefusion Spike of SARS-CoV-2. We used the live attenuated MuV Jeryl Lynn (JL2) strain, a component of the MMR vaccine, as the vector to deliver SARS-CoV-2 spike protein vaccines. We chose two gene junctions, P–M (closer to the 3′ end) and F–SH (closer to the 5′ end), in the MuV genome to insert SARS-CoV-2 S genes, allowing us to compare the expression level of the inserted genes and the viral growth properties. We also compared two forms of stabilized "prefusion" spike in our vaccine constructs (Fig. 1*A*). The first stabilized preS (preS-2P) has two amino acids (K986 and V987) in the S2 portion of the S head region replaced with prolines (2P), the furin cleavage site is deleted to prevent S1–S2 cleavage, and its C-terminal transmembrane/cytoplasmic tail domain is replaced with a T4 fibritin self-trimerizing domain (20), resulting in secretion of preS-2P protein. The second stabilized preS (preS-6P) is similar except that it has six amino acids (K986, V987, F817, A892, A899, and A942) replaced with prolines (HexaPro) (20, 21). preS-6P is expressed more efficiently than preS-2P in eukaryotic expression systems and is more stable at physiological temperatures, and both are more stable than the native S protein (21, 22).

We have developed a yeast-based recombination system for rapid construction of complementary DNA (cDNA) clones of rMuV expressing SARS-CoV-2 S genes (*SI Appendix*, Fig. S1) (23). Using this strategy, we constructed four MuV vaccine vectors with preS-2P or preS-6P inserted at P–M or F–SH gene junctions (Fig. 1*A*). All recombinant viruses were recovered using the standard reverse genetics system and were plaque-purified and sequence-confirmed. Having been thoroughly characterized, the recombinants with preS-2P and preS-6P inserted at the F–SH gene junction were designated as rMuV-preS-2P^{FSH} and rMuV-preS-6P^{FSH}, respectively, and the recombinants with preS-2P and preS-6P inserted at the P–M gene junction were designated as rMuV-preS-2P^{PM} and rMuV-preS-6P^{PM}, respectively.

All recombinant viruses formed significantly smaller plaques in Vero CCL81 cells compared with the parental rMuV (Fig. 1*B*). Recombinant rMuV-preS-2P^{FSH} and rMuV-preS-2P^{PM} formed syncytia similar to rMuV, but syncytia formation by rMuV-preS-6P^{FSH} and rMuV-preS-6P^{PM} was significantly delayed and the resulting syncytia were much smaller (Fig. 1*C* and *SI Appendix*, Figs. S2 and S3). Multistep replication curves showed that these recombinant viruses had delayed replication kinetics but reached similar titers (10^7 plaque-forming units [PFUs] per milliliter) in

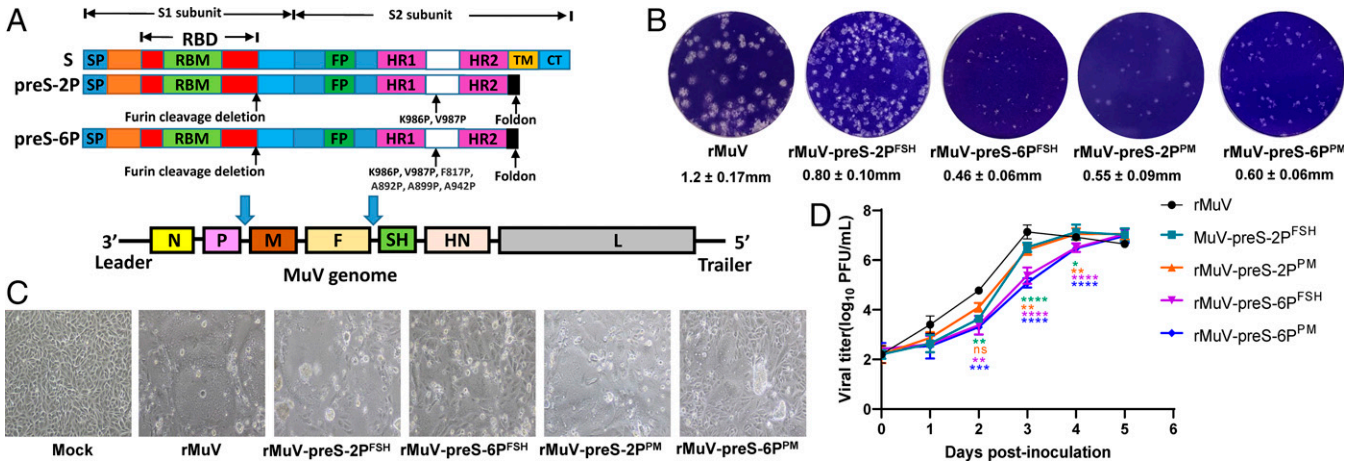

Fig. 1. Recovery and characterization of rMuV expressing the stabilized prefusion spike of SARS-CoV-2. (*A*) Strategy for insertion of preS-2P and preS-6P of SARS-CoV-2 into the MuV genome. The stabilized, prefusion preS-2P and preS-6P genes were inserted into the gene junction between the P and M or F and SH genes in the genome of the MuV JL2 strain using the yeast recombination system. The domain structure of S protein is shown. CT, cytoplasmic tail; FP, fusion peptide; HR, heptad repeat; RBD, receptor-binding domain; RBM, receptor-binding motif; SP, signal peptide; TM, transmembrane domain. The organization of the genes in the negative-sense MuV genome is shown. (*B*) The plaque morphology of rMuVs expressing preS proteins. All plaques were developed after 5 d of incubation. The average diameters of 10 randomly chosen plaques from each virus are shown ± SD. (*C*) rMuVs expressing SARS-CoV-2 preS proteins exhibit delayed syncytia formation in Vero CCL81 cells. An MOI of 0.25 was used for infection. Representative images of syncytia at 72 h are shown. (*D*) Replication kinetics of recombinant viruses in Vero CCL81 cells at an MOI of 0.25. At days 1 to 5, viral titer in cell supernatants was determined by plaque assay. ns, not significant, $*P < 0.05$, $**P < 0.01$, $***P < 0.001$, $****P < 0.0001$.

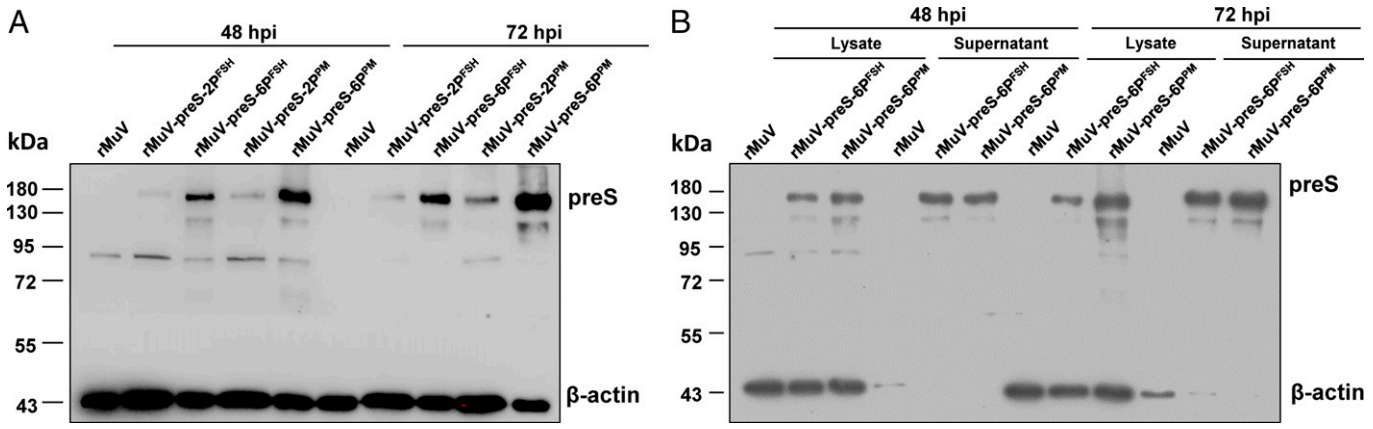

Fig. 2. Characterization of the expression of preS by rMuV vector by Western blot. (*A*) preS protein expression in cell lysates. Vero CCL81 cells were infected with each recombinant virus at an MOI of 0.25. At the indicated time points, cells were lysed in 200 μL of lysis buffer, and lysate was displayed by sodium dodecyl sulfate–polyacrylamide gel electrophoresis and blotted with an anti-RBD protein monoclonal antibody. Cell lysate (20 μL) from rMuV-preS-2P^{FSH} or rMuV-preS-6P^{FSH} and cell lysate (6 μL) from rMuV-preS-2P^{PM} or rMuV-preS-6P^{PM} were analyzed by Western blot. (*B*) preS protein expression in cell lysates and cell-culture medium. Cell lysate (6 μL) and cell-culture supernatant (10 μL) were analyzed by Western blot. hpi, hours postinoculation.

Vero CCL81 cells by day 5 postinoculation (Fig. 1*D*) ($P > 0.05$). These results suggest that insertion of preS-2P and preS-6P genes into the MuV genome attenuates the virus by slowing its replication but does not significantly disturb its final viral titer in cell culture.

SARS-CoV-2 preS Is Highly Expressed by the MuV Vector. The expression of the SARS-CoV-2 preS proteins in rMuV vector–infected cells was examined by immunostaining. rMuV expressed much more preS-6P than preS-2P from both the P–M and F–SH insertion sites (*SI Appendix*, Fig. S4*A*). In addition, expression of SARS-CoV-2 preS-2P or preS-6P from the P–M junction produced more S protein than from the F–SH junction (*SI Appendix*, Fig. S4*A*). Among the four recombinant viruses, rMuV-preS-6P^{PM} had the most abundant S protein expression, while rMuV-preS-2P^{FSH} had the poorest. A similar result was observed at a higher multiplicity of infection (MOI) (1.0) (*SI Appendix*, Fig. S4*B*). rMuV-preS-6P^{PM} produced dramatically more S protein compared with rMuV-preS-2P^{PM} (*SI Appendix*, Fig. S4*B*).

We next performed a Western blot to examine the expression of the S protein. Importantly, rMuV-preS-6P^{PM} had more abundant S protein expression compared with rMuV-preS-2P^{PM}, and rMuV-preS-6P^{FSH} had more abundant S protein expression compared with rMuV-preS-2P^{FSH} (Fig. 2*A* and *SI Appendix*, Fig. S5). As expected, rMuV-preS-6P^{PM} had more abundant S protein expression than rMuV-preS-6P^{FSH}, and rMuV-preS-2P^{PM} had more S protein expression than rMuV-preS-2P^{FSH} in both cell lysates and cell-culture supernatants (Fig. 2 *A* and *B*). Collectively, the expression level of S protein from these four recombinant viruses can be ranked as rMuV-preS-6P^{PM} > rMuV-preS-6P^{FSH} > rMuV-preS-2P^{PM} > rMuV-preS-2P^{FSH}.

Immunogenicity of rMuV-preS-6P^{FSH} in IFNAR1$^{-/-}$ Mice. IFNAR1$^{-/-}$ mice, which lack type I interferon receptor subunit 1 (IFNAR1$^{-/-}$), can be robustly infected by MuV (24). rMuV-preS-2P^{FSH} was excluded from animal studies because it produced little S protein. IFNAR1$^{-/-}$ mice were immunized with either a low dose (4×10^5 PFU) or a high dose (1.0×10^6 PFU) of rMuV-preS-6P^{FSH} and were boosted with the same dose 2 wk later (Fig. 3*A*). A high level of S-specific antibodies was detected in both immunization doses as early as week 2 postimmunization (Fig. 3 *B* and *C*). After booster immunization, antibodies at weeks 5 and 7 further increased. IFNAR1$^{-/-}$ mice immunized with high and low doses had no significant differences in immunoglobulin G (IgG) antibody responses ($P > 0.05$) (Fig. 3*D*). High levels of SARS-CoV-2–specific neutralizing antibody (NAb) were detected at weeks 5 and 7 from the 4×10^5 PFU immunization group (Fig. 3*E*).

At week 7 postimmunization, mice immunized with the low dose (4×10^5 PFU) of rMuV-preS-6P^{FSH} or rMuV were challenged intranasally with 5×10^4 PFU of mouse-adapted (MA) SARS-CoV-2 WA1 strain. As shown in Fig. 3*F*, mice immunized with rMuV-preS-6P^{FSH} did not have significant weight loss ($P > 0.05$) or any clinical signs of illness. However, mice in the rMuV control group had ~20% weight loss by day 4 ($P < 0.0001$) (Fig. 3*F*) and displayed significant signs of illness such as a ruffled coat. The SARS-CoV-2 titer in the lungs of mice in the rMuV-preS-6P^{FSH} group was below the detection limit (Fig. 3*G*). In contrast, ~7.5 $\log_{10}$ PFU per gram of tissue of SARS-CoV-2 was detected in the lungs of mice in the rMuV group ($P < 0.0001$) (Fig. 3*G*). Therefore, these data demonstrate that rMuV-preS-6P^{FSH} is highly immunogenic and provides complete protection against MA SARS-CoV-2 challenge in IFNAR1$^{-/-}$ mice.

rMuV-preS-6P^{FSH} Is Highly Immunogenic in Golden Syrian Hamsters. Golden Syrian hamsters are susceptible to MuV infection (25) and make an excellent animal model for SARS-CoV-2 infection (26, 27). Five 4-wk-old golden Syrian hamsters in each group were first immunized with 1×10^6 PFU of the parental rMuV or rMuV-preS-6P^{FSH}, and boosted with the same dose 2 wk later (Fig. 4*A*). High S-specific enzyme-linked immune absorbent assay (ELISA) antibody titers were detected in all five hamsters in the rMuV-preS-6P^{FSH} group (Fig. 4*B*). A high level of NAbs (average titer of 1,250) in the rMuV-preS-6P^{FSH} group was detected at week 7 (Fig. 4*C*). At week 7, hamsters in the rMuV-preS-6P^{FSH} and rMuV groups were challenged intranasally with 2×10^4 PFU of the SARS-CoV-2 WA1 strain. Hamsters in the rMuV challenge control group exhibited clinical symptoms such as a ruffled coat and weight loss ($P < 0.0001$) (Fig. 4*D*). Importantly, hamsters in the rMuV-preS-6P^{FSH} group did not have any abnormal reaction or weight loss ($P > 0.05$) (Fig. 4*D*). At day 4, all hamsters were killed and lungs and nasal turbinate were collected for virus titration. SARS-CoV-2 titers in lung (Fig. 4*E*) and nasal turbinate (Fig. 4*F*) were near the detection limit in the rMuV-preS-6P^{FSH} group whereas an average titer of 2.4×10^6 and 8.5×10^5 PFU/g of SARS-CoV-2

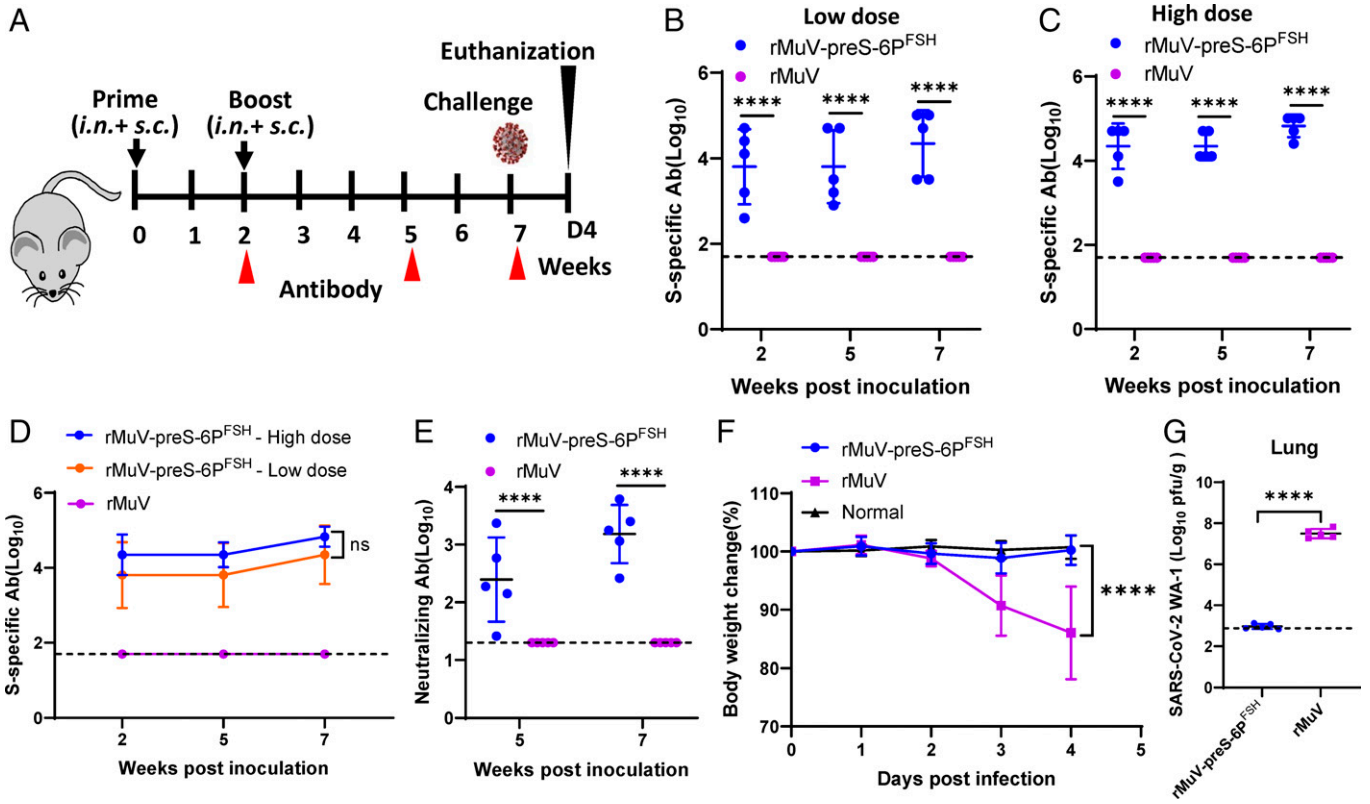

Fig. 3. Immunogenicity of rMuV-preS-6P^{FSH} in IFNAR1$^{-/-}$ mice. (*A*) Immunization schedule. IFNAR1$^{-/-}$ mice ($n = 5$) were immunized with a low (4×10^5 PFU) or a high dose (1×10^6 PFU) of rMuV-preS-6P^{FSH} or rMuV. Two weeks later, mice were boosted with the same virus at the same dose. Serum samples were collected at weeks 2, 5, and 7. i.n., intranasal; s.c., subcutaneous. (*B*) S-specific IgG titer in the 4×10^5 PFU immunization group measured by ELISA. The limit of detection (LoD) is indicated by the dotted line. (*C*) S-specific IgG titer in the 1×10^6 PFU immunization group. (*D*) Comparison of antibody response between low- and high-dose immunization. (*E*) SARS-CoV-2 NAb titers in the 4×10^5 PFU immunization group. Data are expressed as the geometric mean titers (GMTs) of five mice. (*F*) Dynamics of mouse body weight changes after SARS-CoV-2 challenge. Percent of average body weight of five mice ($n = 5$) in each group is shown. (*G*) SARS-CoV-2 titer in lungs. At day 4 after challenge, mice were killed and lungs were collected for virus titration by plaque assay. Viral titers are the GMT of five animals ± SD. The LoD of virus titer in lungs is 2.8 $\log_{10}$ PFU per gram of tissue (dotted line). Data were analyzed using two-way ANOVA and Student's *t* test (****$P < 0.0001$).

was detected in the lungs and nasal turbinate in the rMuV group, respectively. All lungs from the rMuV group developed severe histological lesions (average score of 3.4) including interstitial pneumonia, inflammation, mononuclear cell infiltration, edema, alveolitis, bronchiolitis, and pulmonary hemorrhage. However, lungs from the rMuV-preS-6P^{FSH} group only had mild histological changes (average score of 1.1) such as occasional inflammation and mononuclear cell infiltration (Figs. 4*G* and 5*A* and *SI Appendix*, Fig. S6*A*). Immunohistochemistry (IHC) staining showed that all five lung sections in the rMuV group had extensive N antigen staining, whereas four lung sections were N antigen–negative and one lung section had occasional N antigen spots in the rMuV-preS-6P^{FSH} group (Fig. 5*B* and *SI Appendix*, Fig. S6*B*). These data demonstrate that rMuV-preS-6P^{FSH} vaccination provides near-complete protection against SARS-CoV-2 challenge in hamsters.

rMuV-preS-6P^{PM} Is Significantly More Immunogenic than rMuV-preS-2P^{PM} in IFNAR1$^{-/-}$ Mice. We next compared the immunogenicity of rMuV-preS-2P^{PM} and rMuV-preS-6P^{PM} in IFNAR1$^{-/-}$ mice. Ten IFNAR1$^{-/-}$ mice (five males and five females) per group were immunized with 10^6 PFU of rMuV-preS-2P^{PM}, rMuV-preS-6P^{PM}, or rMuV, and were boosted with the same dose 2 wk later (Fig. 6*A*). All 10 mice in the rMuV-preS-6P^{PM} group developed a high level of S-specific serum IgG antibody at week 2 whereas only 1 of 10 mice in the rMuV-preS-2P^{PM} group was antibody-positive (Fig. 6*B*). The rMuV-preS-6P^{PM} group induced significantly higher serum IgG antibodies than rMuV-preS-2P^{PM} at weeks 2 and 4 although they had a similar level of IgG at week 6 ($P > 0.05$) (Fig. 6*B* and *SI Appendix*, Fig. S7). These data indicate that rMuV-preS-6P^{PM} induced an earlier antibody response that is more potent than rMuV-preS-2P^{PM}.

The five female mice in each group were used for a challenge experiment. The rMuV-preS-6P^{PM} group had 8.5-fold higher NAbs than the rMuV-preS-2P^{PM} group ($P < 0.0001$) at week 6 (Fig. 6*C*) although they had a similar level of serum IgG (*SI Appendix*, Fig. S7*A*). After challenge with MA SARS-CoV-2, mice in the rMuV-preS-6P^{PM} group did not have significant weight loss ($P > 0.05$) (Fig. 6*D*). However, mice in the rMuV-preS-2P^{PM} group had 10% weight loss at day 4 ($P < 0.0001$) compared to normal controls (Fig. 6*D*). After euthanasia, the SARS-CoV-2 titer in the lungs of the rMuV-preS-6P^{PM} group was below the detection limit whereas ~6 $\log_{10}$ PFU per gram of tissue of SARS-CoV-2 was detected in the rMuV-preS-2P^{PM} group (Fig. 6*E*). Therefore, mice immunized with rMuV-preS-6P^{PM} are completely protected against challenge with MA SARS-CoV-2 whereas mice immunized with rMuV-preS-2P^{PM} are only partially protected.

rMuV-preS-6P^{PM} Induces a Higher Mucosal IgA Titer than rMuV-preS-2P^{PM}. The five male mice in the rMuV-preS-2P^{PM} and rMuV-preS-6P^{PM} groups from the experiment above were used for examining S-specific mucosal IgA responses. The NAb titer in the rMuV-preS-6P^{PM} group was significantly higher than the rMuV-preS-2P^{PM} group at week 6 (Fig. 6*F*) although they had a similar level of IgG titers (*SI Appendix*, Fig. S7*B*). At

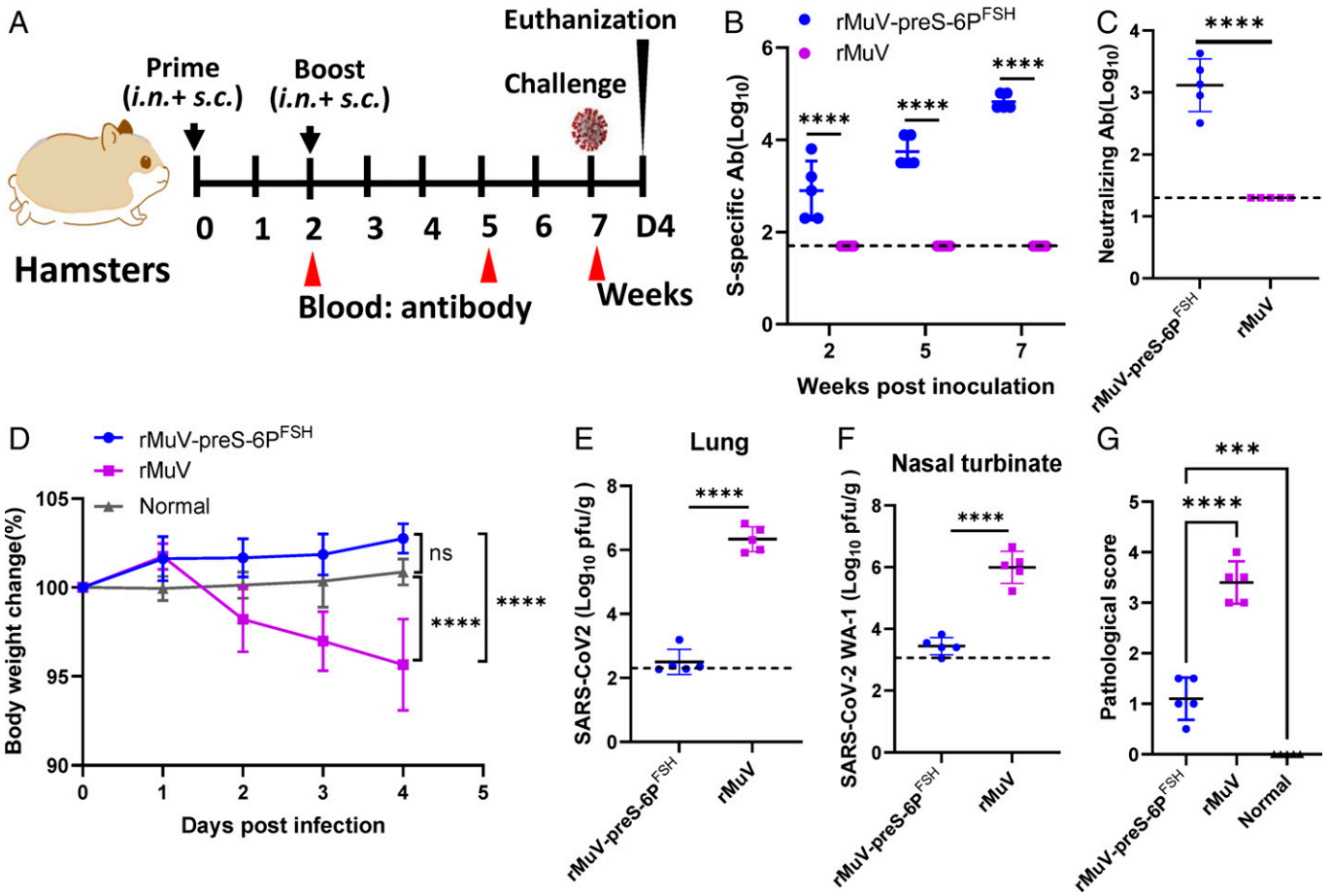

Fig. 4. Immunogenicity of rMuV-preS-6P^{FSH} in golden Syrian hamsters. (*A*) Immunization schedule in hamsters. Four-week-old female golden Syrian hamsters (n = 5) were immunized with 1 × 10^6 PFU (half subcutaneous and half intranasal) of rMuV-preS-6P^{FSH}, parental rMuV, or DMEM. Hamsters were boosted 2 wk later. At weeks 2, 5, and 7, sera were collected for antibody detection. At week 7, hamsters were challenged with 2 × 10^4 PFU of SARS-CoV-2. Unimmunized unchallenged controls were inoculated with DMEM. (*B*) Measurement of SARS-CoV-2 S-specific antibody. The dotted line indicates the limit of detection (LoD). (*C*) Measurement of SARS-CoV-2–specific NAb titer. Data are expressed as GMT of five hamsters. (*D*) Dynamics of hamster body weight changes after SARS-CoV-2 challenge. (*E* and *F*) SARS-CoV-2 titer in lungs (*E*) and nasal turbinate (*F*). At day 4 after challenge, hamsters were killed and lungs and nasal turbinates were collected for virus titration by plaque assay. Viral titers are the GMT of five animals ± SD. The LoD in lung nasal turbinate is 2.2 and 3.0 $\log_{10}$ PFU per gram of tissue (dotted lines). (*G*) Lung pathology score after challenge with SARS-CoV-2 WA1 strain. Each slide was scored based on the severity of histologic changes described previously (24). Score 4, extremely severe; score 3, severe; score 2, moderate; score 1, mild; score 0, no pathological changes. Data were analyzed using two-way ANOVA and Student's t test (***$P < 0.001$, ****$P < 0.0001$).

week 4, three and two mice in the rMuV-preS-6P^{PM} and rMuV-preS-2P^{PM} groups had S-specific saliva IgA antibody, respectively (Fig. 6*G*). Fecal IgA in the rMuV-preS-6P^{PM} group was significantly higher than that in the rMuV-preS-2P^{PM} group (Fig. 6*H*). At week 6, nasal (Fig. 6*I*), saliva (Fig. 6*J*), and fecal (Fig. 6*K*) IgA levels in the rMuV-preS-6P^{PM} group were significantly higher than those in the rMuV-preS-2P^{PM} group. These results indicate that rMuV-preS-6P^{PM} induces a higher level of mucosal IgA antibody responses than rMuV-preS-2P^{PM}.

Immunization with rMuV-preS-2P^{PM} and rMuV-preS-6P^{PM} Induces Th1-Biased T Cell Immune Responses. At week 6, the five male mice in the rMuV-preS-2P^{PM} and rMuV-preS-6P^{PM} groups were killed, and their splenocytes were isolated to characterize vaccine-induced T cells. We first used an enzyme-linked immune absorbent spot (ELISpot) assay to quantify the SARS-CoV-2 S-specific IFN-γ–producing T cells. Upon stimulation with peptide pools spanning the S1 subunit, four out of five mice in the rMuV-preS-6P^{PM} group and all five mice in the rMuV-preS-2P^{PM} group showed an antigen-specific IFN-γ–producing T cell response. However, there was no significant difference between these two groups ($P > 0.05$) (Fig. 7*A*). When the S2 peptide pool or N peptide pool was used for stimulation, the IFN-γ–producing T cell response was barely detectable in either group (Fig. 7*A*). To further characterize the nature of the vaccine-induced T cells, four mice with IFN-γ–producing T cell responses in the rMuV-preS-6P^{PM} group and five mice in the rMuV-preS-2P^{PM} group were analyzed using flow cytometry and intracellular cytokine staining (Fig. 7 *B* and *C* and *SI Appendix*, Fig. S8). After peptide stimulation ex vivo, IFN-γ, tumor necrosis factor-α (TNF-α), and interleukin-2 (IL-2), the signature cytokines of a Th1 response, were detected in CD8+ T cells in both the rMuV-preS-6P^{PM} and rMuV-preS-2P^{PM} groups (Fig. 7*B*). Moreover, S-specific cytokine-producing CD4+ T cells were also detected, and these cells also produced Th1 cytokines IFN-γ, TNF-α, and IL-2, but the frequencies of antigen-specific CD4 T cells were much lower than the antigen-specific CD8 T cells (Fig. 7 *B* and *C*). In both groups, the signature cytokines (such as IL-4, IL-10, and IL-21) produced by Th2 cells were below the detection level (Fig. 7 *B* and *C*). Together, these data suggest that rMuV-based SARS-CoV-2 vaccines, delivered systemically, elicit primarily CD8+ T cell responses.

Hamster Sera Raised by rMuV-preS-6P^{PM} Efficiently Neutralize VoCs. Hamsters were immunized with 10^6 PFU of rMuV-preS-6P^{PM} or rMuV and were boosted with the same dose 2 wk later (Fig. 8*A*). All five hamsters in the rMuV-preS-6P^{PM} group had developed a high level of serum S-specific IgG antibodies,

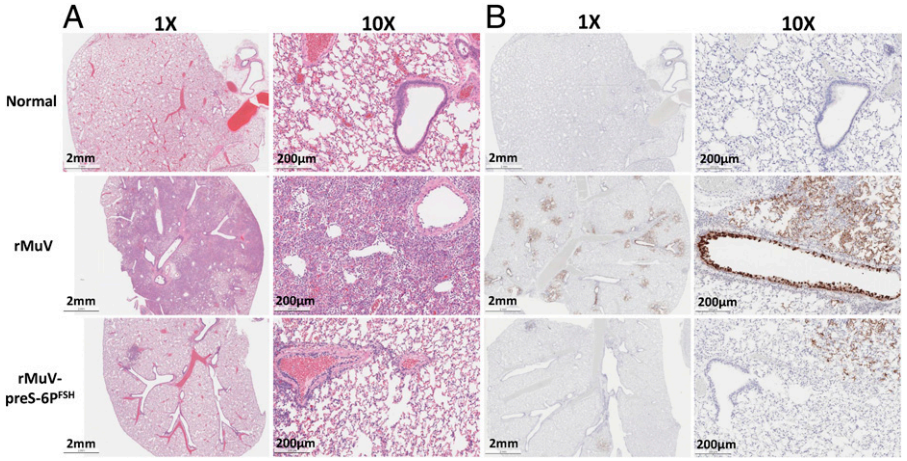

Fig. 5. rMuV-preS-6P^{FSH} immunization protects against lung pathology and virus replication. (*A*) Hematoxylin/eosin staining of lung tissue of hamsters. (*B*) IHC staining of lung tissue of hamsters. Hamsters were killed at day 4 after SARS-CoV-2 WA1 challenge. Anti–SARS-CoV-2 N antibody was used for IHC staining. Micrographs with 1× and 10× magnification of a representative lung section from each group are shown. Scale bars are indicated.

reaching average titers of $10^{4.9}$ and $10^{5.5}$ at week 6, respectively (Fig. 8*B*). Sera at week 6 were chosen to conduct virus-neutralizing assays against SARS-CoV-2 WA1 and VoCs, B.1.1.7, P.1, B.1.617.2, and B.1.351. Importantly, sera raised by rMuV-preS-6P^{PM} neutralized WA1, B.1.1.7, P.1, and B.1.617.2 variants equivalently ($P > 0.05$), but there was a significant reduction in neutralization of the B.1.351 VoC ($P < 0.05$) (Fig. 8*C*). As expected, a high level of S-specific IgA was detected in serum (Fig. 8*D*), saliva (Fig. 8*E*), and vaginal washes (Fig. 8*F*) in the rMuV-preS-6P^{PM} group. These data demonstrate that rMuV-preS-6P^{PM} is highly immunogenic in hamsters and serum raised by rMuV-preS-6P^{PM} is highly potent in neutralizing these VoCs.

Hamsters Immunized with rMuV-preS-6P^{PM} Are Completely Protected against a SARS-CoV-2 Delta Variant Challenge. At week 7 after immunization, hamsters immunized with rMuV-preS-6P^{PM} or rMuV were challenged with 2×10^4 PFU of a SARS-CoV-2 Delta variant strain (Fig. 8*A*). As shown in Fig. 8*G*, hamsters in the rMuV control group had a significant weight loss compared with the mock-infected control group ($P < 0.001$) and exhibited mild clinical signs (such as ruffled fur). In contrast, hamsters in the rMuV-preS-6P^{PM} group did not have any clinical signs or weight loss ($P > 0.05$) (Fig. 8*G*). Importantly, the SARS-CoV-2 titer was below the detection limit in the lungs (Fig. 8*H*) and nasal turbinate (Fig. 8*I*) in the rMuV-preS-6P^{PM}–immunized group. Histological examination showed that all lung tissues from the rMuV group had severe pathological changes (average score of 3.0) while lungs from the rMuV-preS-6P^{PM} group only had mild histological changes (average score of 0.8) (Figs. 8*J* and 9*A* and *SI Appendix*, Fig. S9*A*). IHC staining showed that all five lung sections in the rMuV group had extensive N antigen staining whereas all five lung sections in the rMuV-preS-6P^{PM} group were negative for N antigen (Fig. 9*B* and *SI Appendix*, Fig. S9*B*). Therefore, hamsters immunized with

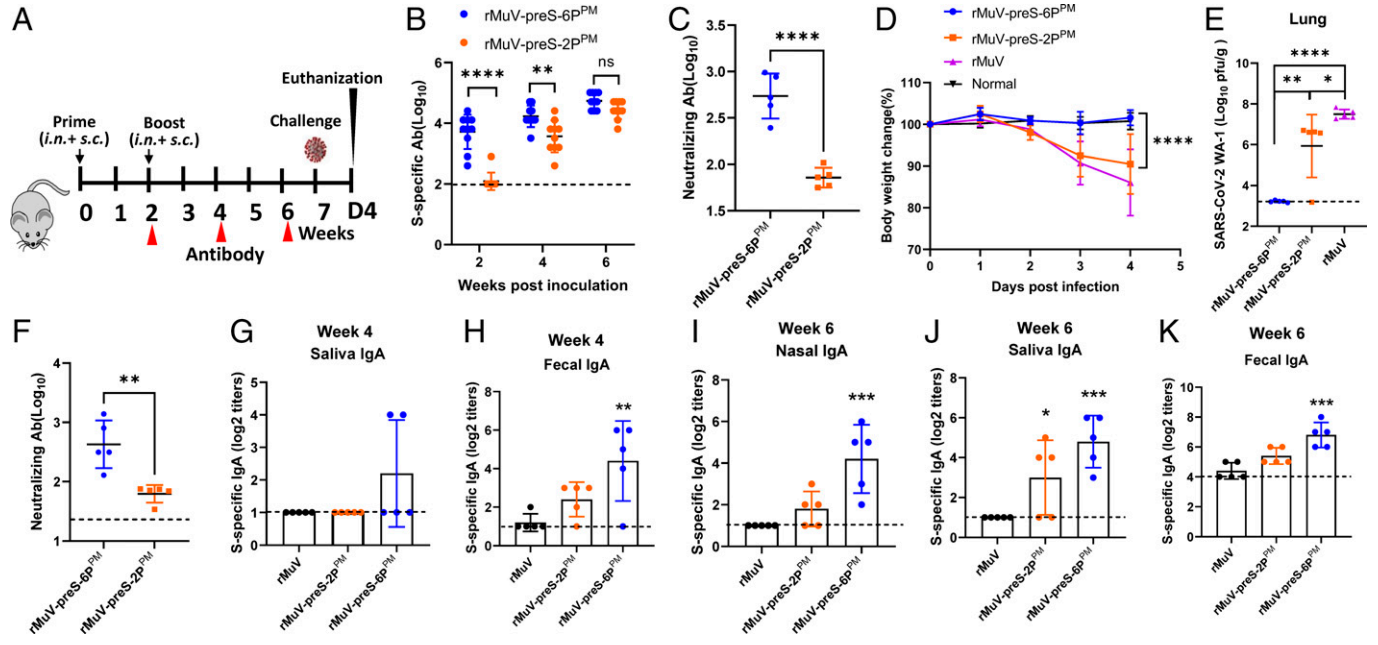

Fig. 6. Comparison of the immunogenicity of rMuV-preS-2P^{PM} and rMuV-preS-6P^{PM} in IFNAR1$^{-/-}$ mice. (*A*) Immunization schedule. IFNAR1$^{-/-}$ mice in group 1 ($n = 10$, 5 male and 5 female), group 2 ($n = 10$, 5 male and 5 female), and group 3 ($n = 5$, female) were immunized with 10^6 PFU (5×10^5 PFU in 20 μL for intranasal and 5×10^5 PFU in 500 μL for subcutaneous) of rMuV-preS-2P^{PM}, rMuV-preS-6P^{PM}, and rMuV, respectively. Group 4 ($n = 5$, female) was inoculated with the same volume of DMEM. Two weeks later, all mice were boosted with the same virus at the same dose and route. (*B*) S-specific IgG titers at weeks 2, 4, and 6 for 10 mice (five female and five male). (*C*) NAb titer at week 6 for five female mice. (*D*) Mouse body weight change after SARS-CoV-2 challenge. At week 7, five female mice in groups 1 to 3 were challenged with 5×10^4 PFU of MA SARS-CoV-2 WA1 strain. (*E*) SARS-CoV-2 titer in lungs. At day 4 after challenge, mice were killed and lungs were collected for virus titration by plaque assay. The LoD in lung is 3.0 $\log_{10}$ PFU per gram of tissue (dotted line). (*F*) NAb titer in five male mice. (*G*) Saliva IgA antibody titer at week 4. (*H*) Fecal IgA antibody titer at week 4. (*I*) Nasal IgA titer at week 6. (*J*) Saliva IgA titer at week 6. (*K*) Fecal IgA antibody titer at week 6. Data were analyzed using two-way ANOVA and Student's *t* test (*$P < 0.05$, **$P < 0.01$, ***$P < 0.001$, ****$P < 0.0001$).

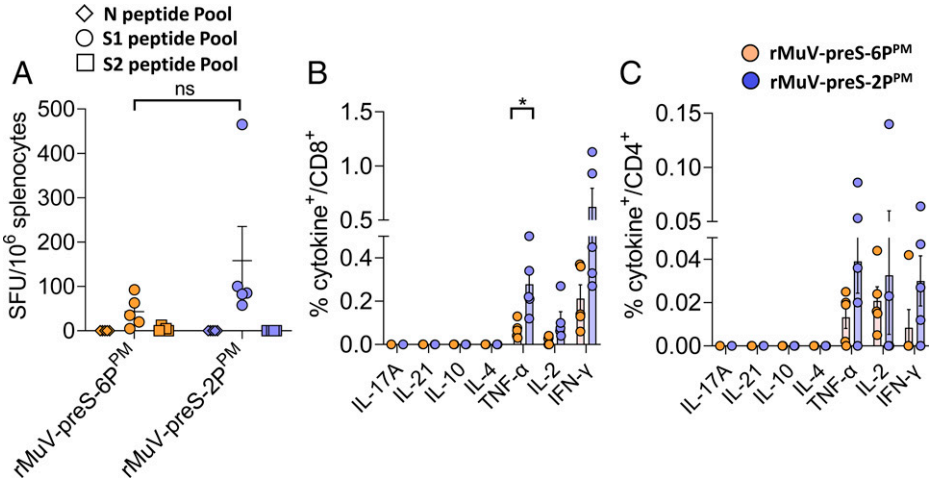

Fig. 7. rMuV-based SARS-CoV-2 induces strong Th1-biased T cell immune responses. (*A*) ELISpot quantification of IFN-γ–producing T cells. Spot-forming units (SFUs) were quantified after the cells were stimulated by peptides representing N (S1 peptides, circles) or C (S2 peptides, boxes) termini of the SARS-CoV-2 spike protein or N peptides. The mean of five mice ± SD is indicated. (*B* and *C*) Cytokine expression in $CD8^+$ (*B*) and $CD4^+$ (*C*) splenocytes. Splenocytes of rMuV-preS-$2P^{PM}$– or rMuV-preS-$6P^{PM}$–vaccinated mice were stimulated ex vivo for 5 h with pools of S1 peptides representing the N terminus of SARS-CoV-2 S protein (5 μg/mL each) in an intracellular cytokine staining assay. Frequencies of $CD4^+$ or $CD8^+$ T cells expressing IFN-γ, TNF-α, or IL-2 are plotted. Data were analyzed using the Student's *t* test (*$P < 0.05$).

rMuV-preS-$6P^{PM}$ were completely protected against challenge with the SARS-CoV-2 Delta variant strain.

Intranasal Immunization with the MuV-Based SARS-CoV-2 Vaccine Induces a Strong Mucosal IgA Response. Recent studies showed that mucosal IgA antibody plays an important role in protecting against SARS-CoV-2 infection (28–31). Thus, we next compared the efficacy of the intranasal and subcutaneous routes for MuV-based SARS-CoV-2 vaccine (Fig. 10*A*). S-specific serum IgG titers in the intranasal group were significantly higher than those in the subcutaneous group ($P < 0.05$) at week 2, but reached similar levels at weeks 4, 6, and 8 (Fig. 10*B*). Importantly, all six mice in the intranasal group generated a high level of S-specific serum IgA antibody at weeks 4, 6, and 8 whereas none of the mice in the subcutaneous group produced an S-specific serum IgA response (Fig. 10*C*). All mice in the intranasal group had S-specific IgA antibody in saliva (Fig. 10*D*) and fecal samples (Fig. 10*E*) at week 6, whereas mice in the subcutaneous group had no S-specific IgA response in the saliva and minimal IgA in feces. Similarly, high levels of saliva (Fig. 10*F*), fecal (Fig. 10*G*), and nasal wash IgA (Fig. 10*H*) were detected in the intranasal group at week 8. Therefore, intranasal delivery of rMuV-preS-$6P^{PM}$ is superior to the subcutaneous route because intranasal immunization induces an earlier IgG antibody response, and a robust IgA antibody response in the serum, as well as in the saliva, feces, and nasal washes.

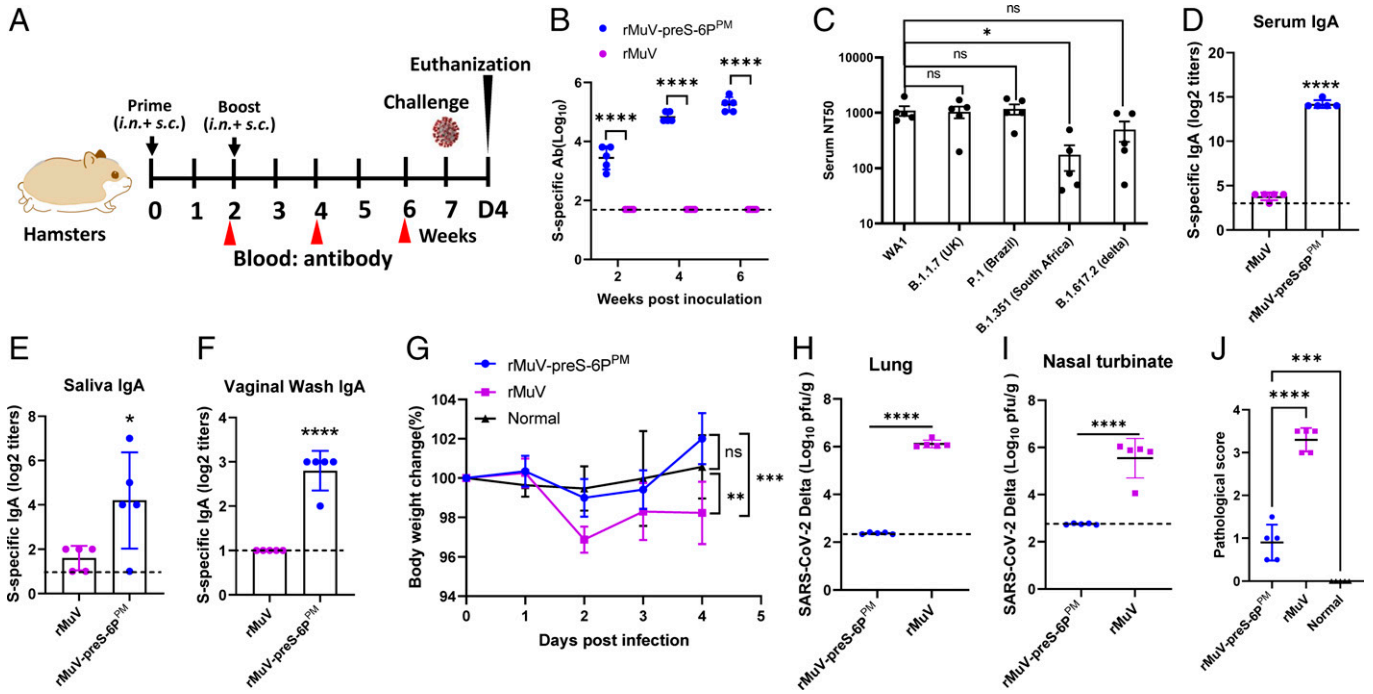

Fig. 8. rMuV-preS-$6P^{PM}$ provides near-complete protection against challenge of the SARS-CoV-2 Delta variant in golden Syrian hamsters. (*A*) Immunization schedule in hamsters. Four-week-old female hamsters ($n = 5$) were immunized with 1×10^6 PFU (half subcutaneous and half intranasal) of rMuV-preS-$6P^{PM}$, parental rMuV, or DMEM. Hamsters were boosted 2 wk later. At weeks 2, 4, and 6, sera were collected for antibody detection. (*B*) Measurement of SARS-CoV-2 S-specific antibody at weeks 2, 4, and 6. (*C*) NAb titer against SARS-CoV-2 VoCs. Sera at week 6 were used for virus-serum neutralization assay. (*D*) Serum IgA titer. (*E*) Saliva IgA titer. (*F*) Vaginal wash IgA titer. (*G*) Dynamics of hamster body weight changes after challenge with the SARS-CoV-2 Delta variant. (*H* and *I*) SARS-CoV-2 titer in lungs (*H*) and nasal turbinate (*I*). At day 4 after challenge, five hamsters from each group were killed and lungs and nasal turbinates were collected for virus titration by plaque assay. Viral titers are the GMT of five animals ± SD. The LoD in lung nasal turbinate is 2.2 and 2.8 $\log_{10}$ PFU per gram of tissue (dotted lines). (*J*) Lung pathology score after challenge with the SARS-CoV-2 Delta variant. Each lung section was scored based on the severity of histologic changes. Score 4, extremely severe; score 3, severe; score 2, moderate; score 1, mild; score 0, no pathological changes. Data were analyzed using two-way ANOVA and Student's *t* test (*$P < 0.05$, **$P < 0.01$, ***$P < 0.001$, ****$P < 0.0001$).

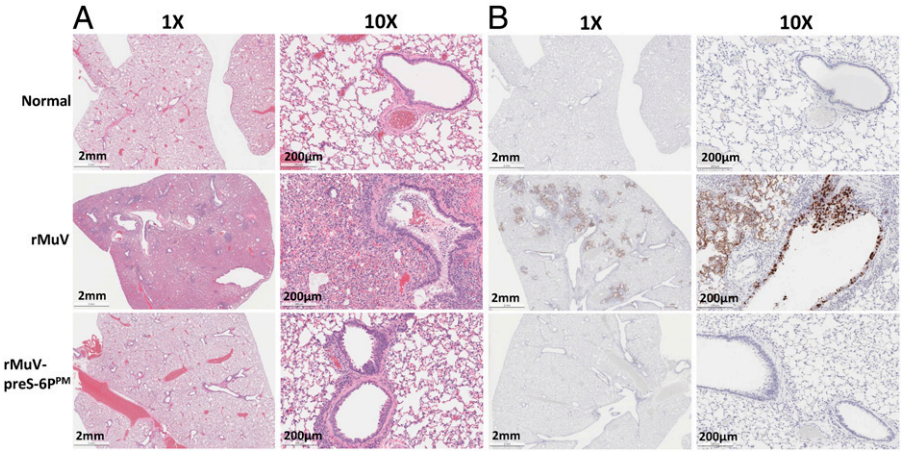

Fig. 9. rMuV-preS-6P^{PM} immunization protects against lung pathology and virus replication. (*A*) Hematoxylin/eosin staining of lung tissue of hamsters. (*B*) IHC staining of lung tissue of hamsters. Hamsters were euthanized at day 4 after SARS-CoV-2 Delta variant challenge. Anti–SARS-CoV-2 N antibody was used for IHC staining. Micrographs with 1× and 10× magnification of a representative lung section from each group are shown. Scale bars are indicated.

Intranasal Immunization Elicits Tissue-Resident Memory T Cell Responses in the Lungs. We next examined the profile of T cell cytokine responses by tissue-resident and circulating T cells in the lungs after intranasal or subcutaneous immunization with the rMuV-based SARS-CoV-2 vaccine. To separate these two T cell populations, anti–CD45-PE was retroorbitally injected into mice 10 min prior to euthanasia. Lungs of rMuV control and immunized mice were dissociated, and lung T cell suspensions were stimulated with phorbol myristate acetate (PMA)/ionomycin, or an S-specific peptide pool, in the presence of protein transport inhibitors. Cells were separated into two pools and surface-stained with antibodies specific for T cell lineages (i.e., CD4 or CD8) and activation status (i.e., CD62L, CD44, CD69), and then fixed, permeabilized, and stained with anti–IFN-γ (for CD8+ T cells) or anti-cytokine antibodies (anti–IFN-γ for CD8+ T cells, or anti–IFN-γ, anti–IL-17, and anti–IL-5 for CD4+ T cells). Cells were analyzed on a Cytek Aurora spectral flow cytometer.

The total percentage (Fig. 11*A*) and number (Fig. 11*E*) of S-specific CD4+CD44+CD62L−CD69+ antigen–experienced T cells increased in mice immunized intranasally, compared with rMuV control or subcutaneously immunized mice. The percentage and number of IFN-γ (Fig. 11 *B* and *F*), IL-17 (Fig. 11 *C* and *G*), or IL-5 (Fig. 11 *D* and *H*)–producing cells also increased in mice immunized by the intranasal route. Separation of the CD45− (tissue-resident) and CD45+ (circulating) T cell populations showed an increase in the percentage and number of CD4+CD44+CD62L−CD69+ cells (*SI Appendix*, Figs. S10 *A* and *E* and S11 *A* and *E*) in both fractions. The percentage and number of IFN-γ (*SI Appendix*, Fig. S11 *B* and *F*), IL-17

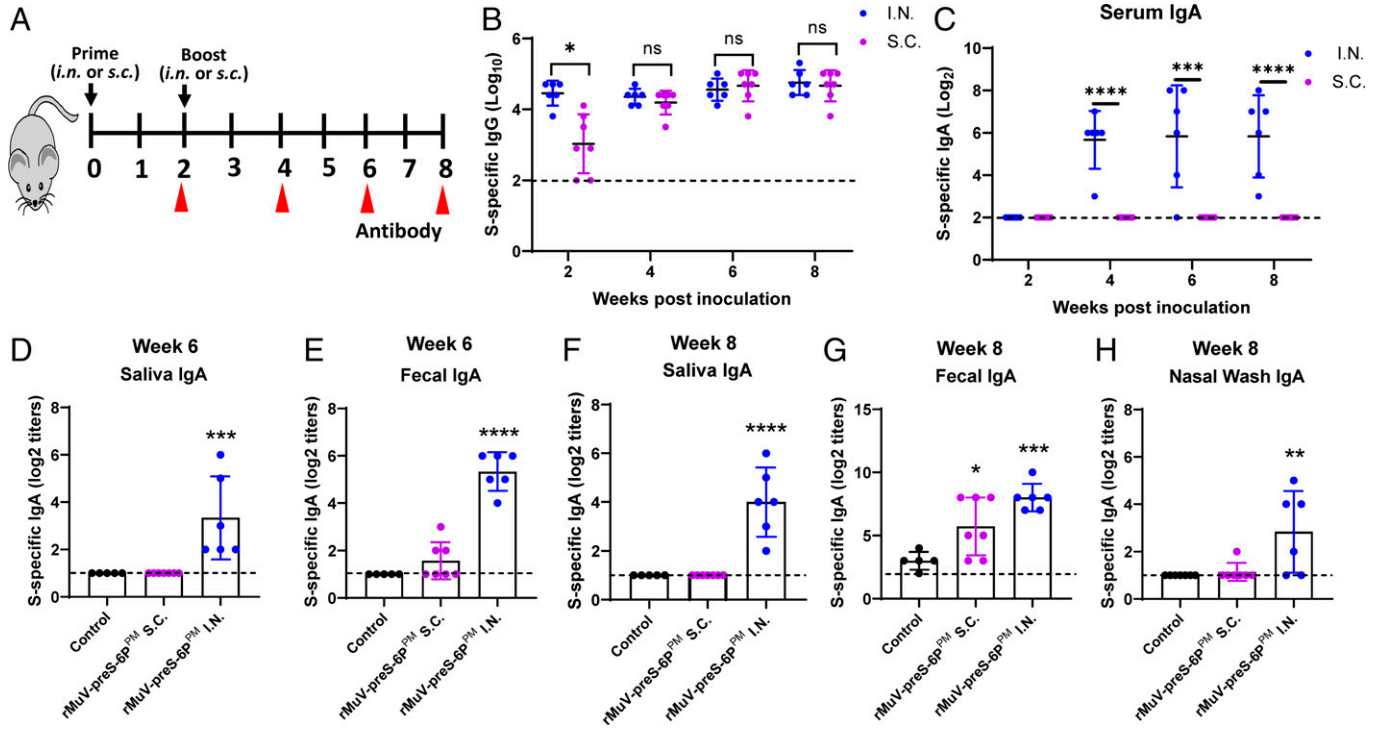

Fig. 10. Intranasal delivery of rMuV-preS-6P^{PM} is superior to the subcutaneous route. (*A*) Immunization schedule. Four-week-old female IFNAR1$^{-/-}$ mice were immunized intranasally or subcutaneously with 10^6 PFU of rMuV-preS-6P^{PM} and were boosted with the same route at the same dose 2 wk later. (*B*) Serum ELISA IgG antibody at weeks 2, 4, 6, and 8. (*C*) Serum IgA antibody at weeks 2, 4, 6, and 8. (*D*) Saliva IgA antibody at week 6. (*E*) Fecal IgA antibody at week 6. (*F*) Saliva IgA antibody at week 8. (*G*) Fecal IgA antibody at week 8. (*H*) Nasal IgA antibody at week 8. Data are the GMT of five animals ± SD. Data were analyzed using two-way ANOVA and Student's *t* test (*$P < 0.05$, **$P < 0.01$, ***$P < 0.001$, ****$P < 0.0001$).

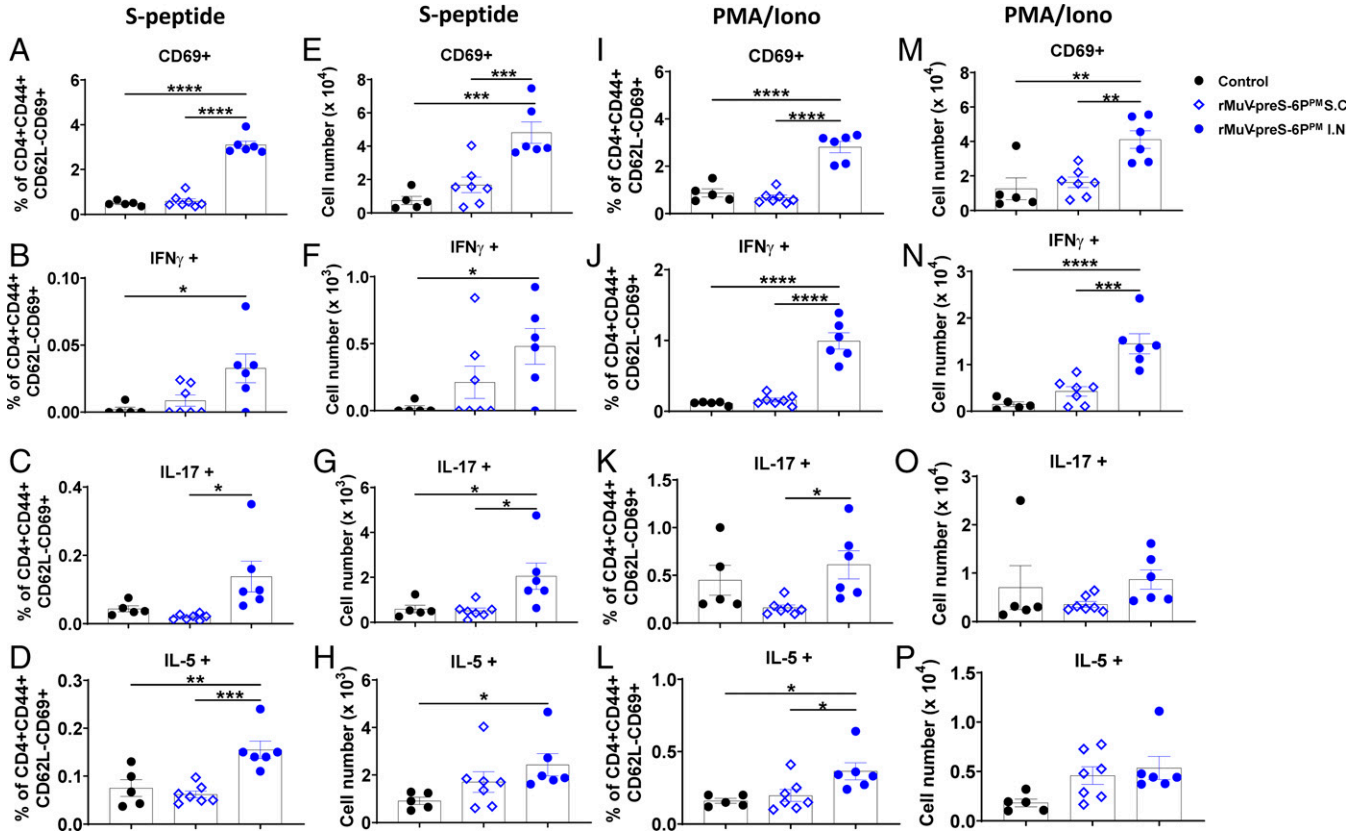

Fig. 11. Intranasal delivery of rMuV-preS-6P^{PM} induces T cell immune response in the lungs. Four-week-old female IFNAR1$^{-/-}$ mice were immunized intranasally or subcutaneously with 10^6 PFU of rMuV-preS-6P^{PM} and boosted with the same route at the same dose 2 wk later. At week 8, mice were injected with CD45-PE antibody 10 min before euthanasia to separate the resident (CD45−) and circulating (CD45+) T cells (*SI Appendix*, Figs. S7 and S8). Lung T cell suspensions were stimulated with an S-specific peptide pool (*A–H*) or PMA/ionomycin (*I–P*) in the presence of protein transport inhibitors. Cells were surface-stained with antibodies specific for CD4 or CD8, CD62L, CD44, and CD69, and then fixed, permeabilized, and stained with anti–IFN-γ, anti–IL-17, and anti–IL-5 for CD4+ T cells. Cells were analyzed on a Cytek Aurora spectral flow cytometer. The percentage (*A–D*) and number (*E–H*) of S-specific total CD4+CD44+CD62L−CD69+ T cells (*A* and *E*) and the subset of IFN-γ+ (*B* and *F*), IL-17+ (*C* and *G*), and IL-5+ (*D* and *H*)–producing CD4+ T cells are shown in *A–H*. The percentage (*I–L*) and number (*M–P*) of PMA-stimulated total CD4+CD44+CD62L−CD69+ T cells (*I* and *M*) and IFN-γ+ (*J* and *N*), IL-17+ (*K* and *O*), and IL-5+ (*L* and *P*)–producing CD4+ T cells are shown in *I–P*. One-way ANOVA with Tukey's multiple comparisons was used to detect differences among groups (*$P < 0.05$, **$P < 0.01$, ***$P < 0.001$, ****$P < 0.0001$).

(*SI Appendix*, Fig. S11 *C* and *G*), and IL-5 (*SI Appendix*, Fig. S11 *D* and *H*)–producing CD45+ cells were significantly higher in intranasally immunized mice, compared with naïve or subcutaneously immunized mice. There was a significant increase in IL-17 (*SI Appendix*, Fig. S10*C*)–producing cells in the CD45− fraction whereas no significant increase in IFN-γ (*SI Appendix*, Fig. S10 *B* and *F*) or IL-5 (*SI Appendix*, Fig. S10 *D* and *H*)–producing cells was observed.

PMA/ionomycin–stimulated cells reflected the same overall pattern, with an increase in the percentage and number of total CD4+CD44+CD62L−CD69+ cells (Fig. 11 *I* and *M*) and IFN-γ (Fig. 11 *J* and *N*), IL-17 (Fig. 11 *K* and *O*), and IL-5 (Fig. 11 *L* and *P*)–producing cells in mice immunized intranasally, compared with naïve or subcutaneously immunized mice. There was a significant increase in CD4+CD44+CD62L−CD69+ cells (*SI Appendix*, Figs. S10 *I* and *M* and S11 *I* and *M*) and IFN-γ (*SI Appendix*, Figs. S10 *J* and *N* and S11 *J* and *N*)–producing cells for both CD45− and CD45+ fractions in mice immunized intranasally whereas no significant increase in IL-17 (*SI Appendix*, Figs. S10 *K* and *O* and S11 *K* and *O*) or IL-5 (*SI Appendix*, Fig. S10 *L* and *P* and S11 *L* and *P*)–producing cells was observed between the three groups.

PMA/ionomycin–stimulated cells showed an increase in the percentage of the CD8+CD44+CD62L−CD69+ fraction (*SI Appendix*, Fig. S12 *A*, *E*, and *I*) in the lungs of intranasally immunized mice, compared with naïve or subcutaneously immunized mice. However, the percentage and number of IFN-γ–producing cells were similar in all groups (*SI Appendix*, Fig. S12 *B–L*).

Together, these data show that intranasal immunization with the MuV-based SARS-CoV-2 vaccine elicits CD4+ T cells in the lungs, with similar proportions of Th1, Th2, and Th17 polarized cells. In contrast, the CD8+ T cell response was less robust, with only a slight increase in CD8+CD69+ cells and the fraction that produced IFN-γ.

Th1 Polarized Systemic T Cell Responses Are Elicited by Subcutaneous Immunization. Spleen cells were isolated from the above mice at week 8 after immunization and were stimulated with purified preS-6P protein. Both intranasal and subcutaneous routes induced a similar level of S-specific CD4+ T cells (*SI Appendix*, Fig. S13*A*). Flow cytometry analysis of CD4+ T cells producing Th1 cytokines revealed that the subcutaneous route stimulated significantly higher IFN-γ and TNF-α responses compared with the intranasal route (*SI Appendix*, Fig. S13 *B* and *C*) ($P < 0.01$). However, neither the intranasal nor the subcutaneous routes induced a significant level of IL-4 or IL-5 (*SI Appendix*, Fig. S13 *D* and *E*), the signature cytokines of Th2 response. In addition, the IL-10 level resulting from the intranasal route was higher than the subcutaneous route (*SI Appendix*, Fig. S13*F*). Neither the intranasal nor the subcutaneous routes induced a significant level of IL-17 (*SI Appendix*, Fig. S13*G*).

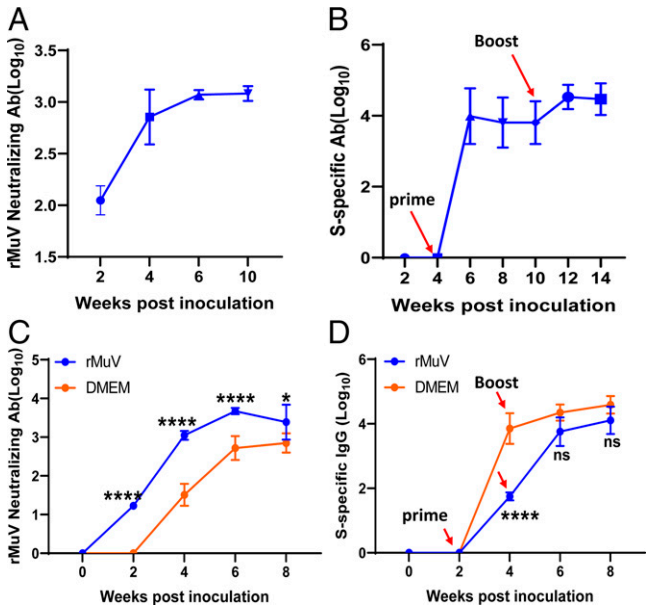

Fig. 12. Effect of preexisting MuV immunity on SARS-CoV-2–specific antibody in hamsters and mice. Four-week-old female golden Syrian hamsters (n = 5) were immunized with 1 × 10^6 PFU (half subcutaneous and half intranasal) of rMuV. Four weeks later, hamsters were immunized with rMuV-preS-6P^{PM}. At week 10, hamsters were boosted with 1 × 10^6 PFU of rMuV-preS-6P^{PM}. Sera were collected every 2 wk for measurement of MuV-specific neutralizing antibody (*A*) and SARS-CoV-2 S-specific serum IgG antibody (*B*). Four-week-old female IFNAR1$^{-/-}$ mice (n = 6) in group 1 were immunized with 1 × 10^6 PFU (half subcutaneous and half intranasal) of rMuV. Mice in the control group (n = 5) were inoculated with DMEM. At week 2, both groups were immunized with 1 × 10^6 PFU of rMuV-preS-6P^{PM}. At week 4, both groups were boosted with 1 × 10^6 PFU of rMuV-preS-6P^{PM}. Sera were collected every 2 wk for measurement of MuV-specific neutralizing antibody (*C*) and SARS-CoV-2 S-specific serum IgG antibody (*D*). Data were analyzed using two-way ANOVA and Student's t test (*P < 0.05, ****P < 0.0001).

Interestingly, IL-21, the signature product of follicular T helper cells, was significantly increased in the intranasal group (P < 0.01) (*SI Appendix*, Fig. S13*H*). We also observed a significant increase in antigen-specific CD8+ T cells in mice immunized by the subcutaneous route (*SI Appendix*, Fig. S13*I*). In addition, intracellular cytokine staining of CD8+ T cells showed that the subcutaneous route stimulated a significantly higher IFN-γ and TNF-α (*SI Appendix*, Fig. S13 *J* and *K*) response than the intranasal route (P < 0.001). These results suggest that systemic T cell responses are elicited by subcutaneous immunization, while intranasal immunization directs the response to the lungs. Furthermore, systemic immunization induces antigen-specific CD4+ and CD8+ T cell responses, while intranasal immunization elicits primarily CD4+ T cell responses.

Induction of SARS-CoV-2–Specific Antibody Responses by rMuV-preS-6P^{PM} in the Presence of Preexisting MuV Immunity. To determine if a MuV-based SARS-CoV-2 vaccine can induce an S-specific immune response in the presence of anti-MuV immunity, hamsters were immunized with 10^6 PFU of the parental MuV JL2 to induce anti-MuV immunity. Four weeks later, these hamsters were immunized with 10^6 PFU of rMuV-preS-6P^{PM}. At week 10, the hamsters were boosted with 10^6 PFU of rMuV-preS-6P^{PM}. All hamsters developed a high level of MuV-specific serum antibody by week 4 (Fig. 12*A*) and the antibody to MuV further increased after immunization with rMuV-preS-6P^{PM}. All hamsters were negative for SARS-CoV-2 S-specific antibodies at weeks 2 and 4 but developed a high level of S-specific antibody at week 6 (week 2 after rMuV-preS-6P^{PM} immunization) and maintained that level through week 10 (Fig. 12*B*). At week 10, hamsters were boosted with rMuV-preS-6P^{PM}, and the S-specific antibodies further increased at weeks 12 and 14 (Fig. 12*B*). These data indicate that rMuV-preS-6P^{PM} is capable of inducing a high level of SARS-CoV-2 S-specific antibodies despite the presence of the preexisting MuV immunity in hamsters.

We also directly compared the S-specific antibody response with or without the preexisting MuV immunity. Briefly, two groups of female IFNAR1$^{-/-}$ mice were inoculated with 10^6 PFU of rMuV (n = 6) or Dulbecco's modified Eagle's medium (DMEM) (n = 5). Two weeks later, both groups were immunized with 10^6 PFU of rMuV-preS-6P^{PM}. At week 4, both groups were boosted with 10^6 PFU of rMuV-preS-6P^{PM}. At weeks 0, 2, 4, 6, and 8, MuV-neutralizing antibody (Fig. 12*C*) and SARS-CoV-2 S-specific IgG antibody were monitored (Fig. 12*D*). Mice immunized with rMuV followed by two doses of rMuV-preS-6P^{PM} induced significantly higher MuV NAb titers than those mice immunized with two doses of rMuV-preS-6P^{PM} (Fig. 12*C*). At week 4, S-specific serum IgG antibodies were detected in both groups; however, S-specific IgG in the DMEM + rMuV-preS-6P^{PM} group was significantly higher than the rMuV + rMuV-preS-6P^{PM} group (P < 0.0001) (Fig. 12*D*). Importantly, both groups reached a similar level of S-specific IgG antibody by weeks 6 and 8 (P > 0.05) (Fig. 12*D*). These results indicate that rMuV-preS-6P^{PM} vaccination is capable of inducing a similar level of S-specific antibody with or without preexisting MuV antibody, although the appearance of S-specific antibody is delayed in the presence of anti-MuV immunity.

Discussion

We have developed an rMuV-based SARS-CoV-2 vaccine candidate. We inserted stabilized versions of the SARS-CoV-2 prefusion S protein, preS-2P or preS-6P, into the P–M or F–SH gene junctions in the MuV genome and found that preS-6P was more efficiently expressed than preS-2P and that preS-6P expression from the P–M gene junction was more efficient than from the F–SH gene junction. Mice and hamsters immunized with rMuV-preS-6P–based SARS-CoV-2 vaccine candidates provided complete protection against challenge with SARS-CoV-2 WA1 and the Delta variant. Furthermore, antibodies induced by this rMuV-preS-6P–based SARS-CoV-2 vaccine efficiently neutralized major VoCs including B.1.1.7, P.1, and B.1.617.2. Intranasal immunization induced robust IgG, mucosal IgA, and systemic and resident T cells. Furthermore, this rMuV-preS-6P–based SARS-CoV-2 vaccine is highly immunogenic, even in the presence of anti-MuV antibody, indicating that rMuV-preS-6P will be effective for all populations regardless of their MuV immunization status. Thus, the rMuV-preS-6P–based SARS-CoV-2 vaccine is a highly promising vaccine candidate that warrants further development.

To our knowledge, only one study has reported the potential use of MuV as a vaccine vector (32). Xu et al. (32) inserted the HIV-1 Gag gene into the MuV genome to generate rMuVgag. Rhesus macaques immunized with rMuVgag and boosted with a recombinant vesicular stomatitis virus (rVSV) expressing HIV-1 Gag (rVSVN4CT1gag1) generated Gag-specific cellular immune responses. Thus, it is not clear whether the Gag-specific cellular immunity observed was due to rMuVgag or rVSVN4CT1gag1. In addition, very low levels of Gag-specific IgG were detected in this prime-boost immunization strategy

(32). The expression of Gag may not have been optimized in this MuV vector.

Here, we optimized the S protein expression in the MuV vector using different gene locations (P–M and F–SH) and different forms of S protein (preS-2P and preS-6P) and demonstrated that the live attenuated MuV JL2 strain is an attractive vector for delivering a SARS-CoV-2 vaccine. Insertion of soluble stabilized SARS-CoV-2 S genes into the MuV JL2 genome slows replication kinetics and results in smaller plaques, which further attenuates this vaccine virus and enhances its safety as a vaccine. Importantly, virus yield (the peak virus titer), though delayed from 3 to 5 d, was similar to the parental rMuV JL2 in Vero CCL81 cells. Finally, the preS-6P protein is highly expressed by the MuV vector and preS-6P is found in both the cell lysate and cell-culture supernatant. Among the tested vaccine candidates, rMuV-preS-6P^{PM} is the best candidate, as it has the highest preS expression and immunogenicity.

Current mRNA vaccines, adenovirus-based vaccines, and recombinant protein–based vaccines employ either full-length native S or preS-2P as antigens (33, 34). We found preS-6P is expressed at dramatically higher amounts than that of preS-2P from either of the gene junctions tested (P–M and F–SH) in the MuV vector, which is similar to the previous observation using a plasmid expression system (21). Mice immunized with rMuV-preS-6P^{PM} had an earlier antibody response than those immunized with rMuV-preS-2P^{PM}. The NAbs and mucosal IgA antibodies elicited by rMuV-preS-6P^{PM} are much higher than those induced by rMuV-preS-2P^{PM}. rMuV-preS-6P^{PM} confers complete protection from SARS-CoV-2 WA1 challenge whereas rMuV-preS-2P^{PM} only provides partial protection. These data demonstrate that rMuV-preS-6P^{PM} is much more immunogenic than rMuV-preS-2P^{PM}. The observation that rMuV-preS-6P^{PM} induces similar levels of IgG antibody but much higher NAbs compared with rMuV-preS-2P^{PM} suggests that preS-6P retains its neutralizing epitopes better than preS-2P. It clearly demonstrates that preS-6P is superior to preS-2P as an antigen for vaccine design. Recently, Sun et al. (35) generated a recombinant Newcastle disease virus (NDV-HXP-S) expressing a membrane-bound prefusion-stabilized spike protein with HexaPro (HXP). NDV-HXP-S was highly immunogenic in mice and hamsters and is currently in clinical trials in Vietnam, Thailand, and Brazil (35).

The emergence of SARS-CoV-2 VoCs complicates the current pandemic. More and more evidence demonstrates that antibodies elicited by the current SARS-CoV-2 vaccines encoding native S or preS-2P have significantly reduced abilities to neutralize these VoCs, particularly for the Delta variant (36, 37) and, more recently, the Omicron (10, 11). Notably, we found that sera raised by rMuV-preS-6P^{PM} neutralized the very similar SARS-CoV-2 WA1 and equally well the B.1.1.7, P.1, and B.1.617.2 variants ($P > 0.05$) although it had significantly reduced neutralizing activity against the B.1.351 variant ($P < 0.05$). In addition, we demonstrate that hamsters immunized with rMuV-preS-6P^{PM} were completely protected from challenge by the Delta variant. These results suggest that a preS-6P vaccine would have a greater ability to neutralize the VoCs than the current native S or preS-2P–based vaccines.

A unique advantage of an rMuV-based SARS-CoV-2 vaccine is that it can be administered intranasally, which efficiently induces local IgA, systemic IgG antibody, and resident T cell–mediated protective immune responses. The respiratory tract is the primary site for SARS-CoV-2 infection. Secretory IgA plays a crucial role in protecting mucosal surfaces against infection by directly impeding SARS-CoV-2 from attaching to cells in the mucosal surface (28–30). Direct comparison of intranasal and subcutaneous routes found that intranasal immunization was not only more effective in inducing IgG antibody but also induced high levels of nasal, fecal, saliva, and serum IgA antibodies and resident and systemic T cell immune responses, whereas subcutaneous immunization induced no or little mucosal IgA response. Furthermore, subcutaneous immunization elicited primarily CD8+ T cells, while intranasal immunization elicited primarily CD4+ T cells in the lungs. This result suggests that CD8+ T cells may be more important for systemic elimination of virally infected cells, while mucosal CD4+ T cells may be important for protection in the respiratory tract.

Although the subcutaneous route is currently used for MMR vaccination in infants and children, intranasal delivery of MuV vaccine has been documented in children and adults (38–40). Interestingly, intranasal vaccination of the MuV L-3 vaccine strain induced the highest rise in MuV-neutralizing antibody titers in human volunteers compared with the other immunization routes (38). Wild-type MuV is highly neurotropic (41, 42). According to the World Health Organization and the US FDA, a nonhuman primate test is required for evaluation of the neurovirulence of MuV vaccines via intracerebral inoculation (41–43). Clearly, both MuV JL1 and MuV JL2 have met the safety requirement (41, 42). Furthermore, insertion of the spike of SARS-CoV-2 further attenuates MuV JL2, thereby enhancing the safety profile. Thus, intranasal delivery of an rMuV-based SARS-CoV-2 vaccine may be a feasible immunization route in humans.

One concern for employing currently used vaccines as vectors for delivering other immunogens is the preexisting antibody to the vector. Most populations have already been immunized with the MMR vaccine and those antibodies might be expected to neutralize a vaccine delivered by MuV, one of the MMR components. However, we found that hamsters with freshly induced, high levels of MuV antibody immunized with rMuV-preS-6P^{PM} generated high levels of S-specific antibody.

Furthermore, we found that rMuV-preS-6P^{PM} vaccination is capable of inducing a similar level of S-specific antibody with or without preexisting MuV antibody in mice, although the appearance of S-specific antibody is delayed in the presence of anti-MuV immunity. This result suggests that the preexisting MuV antibody had a minimal impact on inducing SARS-CoV-2 S-specific antibody in both mice and hamsters.

It has been speculated that the MMR vaccine, itself, may protect against or reduce the severity of SARS-CoV-2 infection in humans (44–47). Gold et al. (48) reported that several countries with recent, large-scale MMR vaccination campaigns had the fewest COVID-19 deaths and that there is a significant inverse correlation between MuV antibody titers from MMR vaccination and COVID-19 severity. If true, immunization with a MuV-based SARS-CoV-2 vaccine might offer this additional benefit. Although we did not directly compare disease severity between phosphate-buffered saline–inoculated and rMuV-immunized mice and hamsters after SARS-CoV-2 challenge, our results clearly showed that immunization with the control rMuV vector was not protective against a large dose of SARS-CoV-2 WA1 or the Delta variant.

In summary, we have developed a highly efficacious rMuV-vectored preS-6P vaccine candidate that induces a broad neutralizing antibody against VoCs and provides complete protection against SARS-CoV-2 WA1 and Delta variant challenge in animal models. Thus, the rMuV-based preS-6P vaccine is a promising vaccine candidate, warranting further development as a COVID-19 vaccine. By incorporating rMuV-preS-6P into the existing MMR vaccine, a

quadruple vaccine could be developed against these four important childhood pathogens.

Materials and Methods

All animals were housed within University Laboratory Animal Resources facilities of The Ohio State University under approved Institutional Laboratory Animal Care and Use Committee guidelines (protocol no. 2009A1060-R3 and 2020A00000053). Detailed descriptions of cell cultures, virus strains, construction of infectious cDNA clones of MuV, recovery and characterization of rMuV expressing SARS-CoV-2 S proteins, multistep growth curves, preparation of large stocks of rMuVs, MuV and SARS-CoV-2 plaque assays, Western blot, immunostaining, RNA extraction, RT-PCR, animal studies in IFNAR1$^{-/-}$ mice and golden Syrian hamsters, purification of S protein and S peptides, T cell assay, ELISpot assay, quantification of intracellular cytokine production, flow cytometry analysis, detection of SARS-CoV-2–specific IgG and IgA antibodies by ELISA, detection of SARS-CoV-2– and MuV-neutralizing antibody, determination of SARS-CoV-2 titer in mice and hamster tissues, histology, immunohistochemical staining (IHC), and statistical analysis are provided in *SI Appendix*.

Data Availability. All study data are included in the article and/or *SI Appendix*.

ACKNOWLEDGMENTS. This study was in part supported by grants from the NIH (R01AI090060 to J.L.; P01 AI112524 to M.E.P. and J.L.; RM1 HG008935 to J.L.; and U19AI42733 to M.E.P.). P.N.B. was supported by NIH Grants R01AI145144 and R01AI157205, and A.K. was supported by NIH Grants R01AI137567 and R01AI151175. The study was also supported by startup fund and bridge funding (J.L.) from the Department of Veterinary Biosciences, College of Veterinary Medicine at The Ohio State University and a seed grant (M.E.P. and J.L.) from the Abigail Wexner Research Institute at Nationwide Children's Hospital. We thank Jason McLellan (University of Texas at Austin) for providing plasmids for expressing both of the stabilized prefusion spike proteins for this study. We thank the BSL3 working group at The Ohio State University for their support for this study. We also thank Sally L. Li at Columbus Academy for drawing cartoon images of a mouse and hamster for figures.

Author affiliations: [a]Department of Veterinary Biosciences, The Ohio State University, Columbus, OH 43210; [b]Center for Vaccines and Immunity, Abigail Wexner Research Institute, Nationwide Children's Hospital, Columbus, OH 43205; [c]Department of Microbial Infection and Immunity, College of Medicine, The Ohio State University, Columbus, OH 43210; [d]Department of Disease Intervention and Prevention, Texas Biomedical Research Institute, San Antonio, TX 78227; [e]Infectious Disease Institute, The Ohio State University, Columbus, OH 43210; and [f]Department of Pediatrics, College of Medicine, The Ohio State University, Columbus, OH 43210

Author contributions: Y.Z., M.L., M.M.S., A.K., L.M.-S., P. Dubey, P.N.B., M.E.P., and J.L. designed research; Y.Z., M.L., M.K.C., E.K., M.M.S., C.Y., P. Dravid, M.C., J.-G.P., J.M.H., S.T., S.C., A.D.K., S.S.M., H.S., X.L., and J.L. performed research; Y.Z., J.S.Y., and J.L. contributed new reagents/analytic tools; Y.Z., M.L., M.K.C., E.K., M.M.S., C.Y., P. Dravid, M.C., J.-G.P., J.M.H., S.T., S.S.M., H.S., X.L., A.K., L.M.-S., P. Dubey, P.N.B., M.E.P., and J.L. analyzed data; Y.Z., M.L., and J.L. wrote the paper; J.L. oversaw the project; and J.L. obtained funding.

1. Q. Li *et al.*, Early transmission dynamics in Wuhan, China, of novel coronavirus-infected pneumonia. *N. Engl. J. Med.* **382**, 1199–1207 (2020).
2. C. Huang *et al.*, Clinical features of patients infected with 2019 novel coronavirus in Wuhan, China. *Lancet* **395**, 497–506 (2020).
3. N. Zhu *et al.*; China Novel Coronavirus Investigating and Research Team, A novel coronavirus from patients with pneumonia in China, 2019. *N. Engl. J. Med.* **382**, 727–733 (2020).
4. C. Lucas *et al.*; Yale SARS-CoV-2 Genomic Surveillance Initiative, Impact of circulating SARS-CoV-2 variants on mRNA vaccine-induced immunity. *Nature* **600**, 523–529 (2021).
5. A. T. Widge *et al.*; mRNA-1273 Study Group, Durability of responses after SARS-CoV-2 mRNA-1273 vaccination. *N. Engl. J. Med.* **384**, 80–82 (2021).
6. J. T. Heggestad *et al.*, Rapid test to assess the escape of SARS-CoV-2 variants of concern. *Sci. Adv.* **7**, eabl7682 (2021).
7. C. Fenwick *et al.*, A high-throughput cell- and virus-free assay shows reduced neutralization of SARS-CoV-2 variants by COVID-19 convalescent plasma. *Sci. Transl. Med.* **13**, eabi8452 (2021).
8. K. B. Pouwels *et al.*, Effect of Delta variant on viral burden and vaccine effectiveness against new SARS-CoV-2 infections in the UK. *Nat. Med.* **27**, 2127–2135 (2021).
9. Z. Liu *et al.*, Identification of SARS-CoV-2 spike mutations that attenuate monoclonal and serum antibody neutralization. *Cell Host Microbe* **29**, 477–488.e4 (2021).
10. L. Lu *et al.*, Neutralization of SARS-CoV-2 Omicron variant by sera from BNT162b2 or Coronavac vaccine recipients. *Clin. Infect. Dis.*, 10.1093/cid/ciab1041 (2021).
11. K. Kupferschmidt, G. Vogel, How bad is Omicron? Some clues are emerging. *Science* **374**, 1304–1305 (2021).
12. K. R. Woodworth *et al.*, The Advisory Committee on Immunization Practices' interim recommendation for use of Pfizer-BioNTech COVID-19 vaccine in children aged 5–11 years–United States, November 2021. *MMWR Morb. Mortal. Wkly. Rep.* **70**, 1579–1583 (2021).
13. E. B. Walter *et al.*, Evaluation of the BNT162b2 Covid-19 vaccine in children 5 to 11 years of age. *N. Engl. J. Med.* **386**, 35–46 (2022).
14. W. W. Lin *et al.*, A durable protective immune response to wild-type measles virus infection of macaques is due to viral replication and spread in lymphoid tissues. *Sci. Transl. Med.* **12**, eaax7799 (2020).
15. W. J. Moss, D. E. Griffin, Measles. *Lancet* **379**, 153–164 (2012).
16. F. Kauffmann *et al.*, Measles, mumps, rubella prevention: How can we do better? *Expert Rev. Vaccines* **20**, 811–826 (2021).
17. C. J. Sauder *et al.*, Evidence that a polyhexameric genome length is preferred, but not strictly required, for efficient mumps virus replication. *Virology* **493**, 173–188 (2016).
18. I. Almansour, Mumps vaccines: Current challenges and future prospects. *Front. Microbiol.* **11**, 1999 (2020).
19. E. Lam, J. B. Rosen, J. R. Zucker, Mumps: An update on outbreaks, vaccine efficacy, and genomic diversity. *Clin. Microbiol. Rev.* **33**, e00151-19 (2020).
20. D. Wrapp *et al.*, Cryo-EM structure of the 2019-nCoV spike in the prefusion conformation. *Science* **367**, 1260–1263 (2020).
21. C. L. Hsieh *et al.*, Structure-based design of prefusion-stabilized SARS-CoV-2 spikes. *Science* **369**, 1501–1505 (2020).
22. J. McLellan, Structure-based design of prefusion-stabilized SARS-CoV-2 spikes. *Acta Crystallogr. A Found. Adv.* **76**, 209 (2020).
23. M. Lu *et al.*, A safe and highly efficacious measles virus-based vaccine expressing SARS-CoV-2 stabilized prefusion spike. *Proc. Natl. Acad. Sci. U.S.A.* **118**, e2026153118 (2021).
24. A. Pickar *et al.*, Establishing a small animal model for evaluating protective immunity against mumps virus. *PLoS One* **12**, e0174444 (2017).
25. J. S. Wolinsky, J. M. Kelly III, J. R. Baringer, Ultrastructure of mumps virus replication in organotypic cultures of hamster choroid plexus. *J. Gen. Virol.* **30**, 197–205 (1976).
26. S. F. Sia *et al.*, Pathogenesis and transmission of SARS-CoV-2 in golden hamsters. *Nature* **583**, 834–838 (2020).
27. M. Lu *et al.*, A methyltransferase-defective vesicular stomatitis virus-based SARS-CoV-2 vaccine candidate provides complete protection against SARS-CoV-2 infection in hamsters. *J. Virol.* **95**, e0059221 (2021).
28. E. Kim *et al.*, Inhibition of elastase enhances the adjuvanticity of alum and promotes anti-SARS-CoV-2 systemic and mucosal immunity. *Proc. Natl. Acad. Sci. U.S.A.* **118**, e2102435118 (2021).
29. D. Sterlin *et al.*, IgA dominates the early neutralizing antibody response to SARS-CoV-2. *Sci. Transl. Med.* **13**, eabd2223 (2021).
30. L. Sun *et al.*, Increased in vitro neutralizing activity of SARS-CoV-2 IgA1 dimers compared to monomers and IgG. *Proc. Natl. Acad. Sci. U.S.A.* **118**, e2107148118 (2021).
31. S. Terreri *et al.*, Persistent B cell memory after SARS-CoV-2 vaccination is functional during breakthrough infections. *Cell Host Microbe* **30**, 400–408.e4 (2022).
32. R. Xu *et al.*, Prime-boost vaccination with recombinant mumps virus and recombinant vesicular stomatitis virus vectors elicits an enhanced human immunodeficiency virus type 1 Gag-specific cellular immune response in rhesus macaques. *J. Virol.* **83**, 9813–9823 (2009).
33. M. Lipsitch, F. Krammer, G. Regev-Yochay, Y. Lustig, R. D. Balicer, SARS-CoV-2 breakthrough infections in vaccinated individuals: Measurement, causes and impact. *Nat. Rev. Immunol.* **22**, 57–65 (2022).
34. F. Amanat *et al.*, Introduction of two prolines and removal of the polybasic cleavage site lead to higher efficacy of a recombinant spike-based SARS-CoV-2 vaccine in the mouse model. *mBio* **12**, e02648-20 (2021).
35. W. Sun *et al.*, A Newcastle disease virus expressing a stabilized spike protein of SARS-CoV-2 induces protective immune responses. *Nat. Commun.* **12**, 6197 (2021).
36. B. Ying *et al.*, Protective activity of mRNA vaccines against ancestral and variant SARS-CoV-2 strains. *Sci. Transl. Med.* **14**, eabm3302 (2022).
37. R. E. Chen *et al.*, In vivo monoclonal antibody efficacy against SARS-CoV-2 variant strains. *Nature* **596**, 103–108 (2021).
38. V. P. Krasnova, N. V. Iuminova, V. A. Liashenko, An intranasal method of revaccination against mumps [in Russian]. *Vopr. Virusol.* **39**, 24–26 (1994).
39. P. L. Ogra, Y. Chiba, K. R. Beutner, A. Morag, Vaccination by non-parenteral routes: Characteristics of immune response. *Dev. Biol. Stand.* **33**, 19–26 (1976).
40. N. V. Iuminova, V. P. Krasnova, V. A. Liashenko, The specific activity and immunological safety of a live mumps vaccine from the Leningrad-3 strain in intranasally revaccinated adult subjects [in Russian]. *Vopr. Virusol.* **39**, 113–116 (1994).
41. S. A. Rubin, M. A. Afzal, Neurovirulence safety testing of mumps vaccines–Historical perspective and current status. *Vaccine* **29**, 2850–2855 (2011).
42. S. A. Rubin *et al.*, The mumps virus neurovirulence safety test in rhesus monkeys: A comparison of mumps virus strains. *J. Infect. Dis.* **180**, 521–525 (1999).
43. O. Maximova *et al.*, Monkey neurovirulence test for live mumps vaccine. *Biologicals* **24**, 223–224 (1996).
44. Ö. Özdemir, Measles-mumps-rubella vaccine and COVID-19 relationship. *mBio* **11**, e01832-20 (2020).
45. M. Taheri Soodejani, M. Basti, S. M. Tabatabaei, K. Rajabkhah, Measles, mumps, and rubella (MMR) vaccine and COVID-19: A systematic review. *Int. J. Mol. Epidemiol. Genet.* **12**, 35–39 (2021).
46. E. Marakasova, A. Baranova, MMR vaccine and COVID-19: Measles protein homology may contribute to cross-reactivity or to complement activation protection. *mBio* **12**, e03447-20 (2021).
47. J. W. Ashford *et al.*, MMR vaccination: A potential strategy to reduce severity and mortality of COVID-19 illness. *Am. J. Med.* **134**, 153–155 (2021).
48. J. E. Gold *et al.*, Analysis of measles-mumps-rubella (MMR) titers of recovered COVID-19 patients. *mBio* **11**, e02628-20 (2020).